As originally published in the SMTA Proceedings.

Effect of Bi-Addition on the High Strain Rate Properties of SnAgCu Solders under Wide Temperature Extremes and Prolonged Exposure to High Temperature

Pradeep Lall, Vishal Mehta, Mrinmoy Saha
Auburn University
NSF-CAVE3 Electronics Research Center
Auburn, AL 36849
E-mail: lall@auburn.edu
Tele: +1(334)844-3424

ABSTRACT
The use of constitutive models is essential in ensuring the reliability and safety of high-reliability electronics systems, particularly those designed for use in harsh environments. These systems can experience extreme temperatures, ranging from -65°C to +200°C, that can cause significant out-of-plane deformation of board assemblies when exposed to shock, vibration, or transient loads. In applications such as automotive and aerospace, electronics may require prolonged high-temperature exposure in the range of 150-200°C and random exposure to mechanical shock and vibration. Additionally, electronics may be stored for extended periods in non-climate-controlled enclosures before deployment. To address the negative effects of sustained high-temperature exposure, the industry has experimented with the addition of dopants to SAC solders. This study examines various doped alloys, including SAC-Q, SAC-R, M758, and SAC305 solder, in a strain-rate range of 1-100 per second in the temperature range of -65°C to +200°C after one year of sustained exposure to 50°C and 100°C. The study also involves the use of dopants such as Nickel and Bismuth. The Anand parameters have been computed and used to quantify the accuracy of the Anand model by comparing the experimentally measured data with the predicted data with the computed model constants. Moreover, the Anand parameters have been integrated into an FE framework to simulate drop events for a ball-grid array package on a printed circuit board assembly, aiming to determine the hysteresis loop and plastic work density. The study also examines the evolution in hysteresis loops and PWD.

Keywords: Un-doped and doped Lead-Free Solders, High Strain Rates, Anand Viscoplasticity Model, FE analysis for drop/shock.

INTRODUCTION

High-reliability electronic systems used in automotive underhood and aerospace electronics may face challenges such as extended storage, low operating temperatures, and high strain rates. To ensure their dependability, it is important to use constitutive models to analyze and evaluate them. These electronic systems may have to operate in harsh environments and be subjected to negative temperatures ranging from 0°C to -65°C. When exposed to rapid loads or vibrations, the board assemblies may deform considerably out-of-plane, causing significant damage over their operational life. Previous studies have shown that electronic vehicle systems installed underhood, on the engine driver interior, and in the ECU box can be exposed to temperatures ranging from -40°C to +200°C [1]. SAC solders have shown the evolution of mechanical properties at low strain rates after moderate sustained temperature exposure. However, quantifying the expected degradation in mechanical properties and identifying failure thresholds are crucial in ensuring high reliability.

Solder companies are seeking ways to mitigate the long-term impact of high-temperature exposure on the mechanical properties of SnAgCu solders. Previous studies have examined the characteristics of SAC solder alloys under varying thermal loads and strain rates, ranging from 10^{-6} to 10^{-1} per second. Researchers have also explored the effects of thermal aging [4]-[15]. Wong's findings revealed that 63Sn37Pb is less susceptible to strain rate in comparison to lead-free solder alloys [16]. In an earlier study, authors [7]-[15] focused on the material behavior of several SAC materials under different strain conditions due to thermal aging. However, there is limited information on new formulations' mechanical performance, reliability, and constitutive models. The impact of sustained exposure to high temperatures on the high strain rate constitutive behavior is unknown. Currently, mechanical characteristics at low strain rates have only been evaluated in material test/experiment systems. This paper focuses specifically on the effects of sustained high temperatures on the high strain rate of doped lead-free solders operating between -65°C to 200°C. The study covers a range of strain rates from 1-100s^{-1}.

In the field of electronic packaging, finite element modeling has been widely used for designing solder joint attachments. In order to accurately capture the non-linear behavior of solder alloys, various material models have been employed such as elastic, elastic-plastic, creep, and viscoplasticity. The Anand model is one of the frequently used models to describe the non-linear behavior of solder materials, as demonstrated in previous studies [4]-[15] and [17]-[19]. Amagai [19] proposed a modified Anand Constitutive model for lead-free solders Sn3.5Ag0.75Cu and SAC105 (Snl.0Ag0.5Cu), which provided values for the Anand model constants. Motalab's research showed that long-term thermal aging of mechanical properties in lead-free alloys can indicate thermal fatigue at lower strain rates [6].

The current research aims to fill a gap in the state of the art by measuring the characteristics of alloys such as SAC305, SAC-Q, M758, and SAC-R at low temperatures ranging from -65°C to 200°C, high strain rates, and varying periods of thermal

aging of up to 1 year, at 50°C and 100°C. To provide a comprehensive understanding of the material's behavior across the entire temperature range and strain rates, the Anand Viscoplasticity model constants have been calculated. Furthermore, a quantitative analysis of the model constants' evolution during thermal storage at high temperatures has been conducted. The accuracy of the model has been assessed by comparing the measured material and anticipated deformation behavior using the derived model constants.

SAMPLE FABRICATION

EDX analysis was conducted to extract the chemical composition of three types of solder alloys: SAC305, SAC-Q, and SAC-R. To create the SAC solder specimens, small pieces of the alloys were melted in a glass crucible tube. The rectangular samples were created using precise rectangular cross-section glass tubes and a vacuum pump. Table 1 presents the results of this investigation.

Table 1. SAC Solder's Composition

	% Content			
Element	***SAC305***	***SAC-Q***	***M758***	***SAC-R***
Sn	96.5	91.6	92.6	96.62
Ag	3.0	2.9	2.4	0.00
Cu	0.5	0.7	0.8	0.92
Bi	0.0	3.0	4.0	2.46
Ni	0.0	0.0	0.2	0.00

The sample has a thickness of 0.5 mm, which is comparable to the height of solder junctions used in fine pitch electronics. The glass tubes are cooled using the water quenching process and once solidified, the specimen is reflowed in the Heller 1800EXL nine-zone reflow oven. To minimize the effect of room temperature aging, test samples were immediately cooled to room temperature and placed in an isothermal oven for isothermal aging. Samples marked with SAC305 and M758 were aged for up to 1 year at 100°C, while SAC-Q and SAC-R samples were aged at 50°C for up to 1 year. To detect any flaws or damages before the tensile test, test samples were taken out of the glass tubes, and X-ray images were captured. The sample preparation method and images are explained in detail in the author's previous publications [15].

EXPERIMENTAL SETUP

The study involved testing specimens with various standardized strain rates using an impact hammer-based method. Two high-speed cameras were used to record data on the strain and deformation of the solder specimen. High strain rates and extreme testing temperatures (ranging from -65 to 200°C) were applied to measure stress-strain data. To achieve low testing temperatures, a cooling chamber was introduced to the tensile test setup, with liquid nitrogen being pumped through it. The setup ensures a steady strain rate throughout the entire test. Two grips were used to secure the test sample, and a load cell was added to the top of the upper grip to measure the tensile load during testing. The experiment setup also included two high-speed cameras to monitor the movement of the test sample and impact hammer. The authors have previously published detailed works that explain the sample fabrication and the experimental setup. [7]- [15].

EXPERIMENTAL MATRIX AND TEST DATA

Table 2 lists several test conditions, and each one was tested using five samples with the impact hammer-based tensile setup. To create each stress-strain curve, the results of five separate samples were averaged. The study measured the effects of low operating temperatures, high strain rates, and thermal aging conditions on the characteristics of the extracted materials.

Table 2. Test Matrix for SAC-Q, SAC305, SAC-R, M758 Solders

Operating Temperatures: -65 to 200°C Strain Rates: 10, 35, 50, 75 per sec								
Material	**Aging Temp.**	**Aging Duration (in Days)**						
		0	***30***	***60***	***120***	***180***	***240***	***360***
SAC-Q	**50 °C**	X	X	X	X	X	X	X
SAC305	**100 °C**	X	X	X	X	X	X	X
M758	**100 °C**	X	X	-	-	X	-	X
SAC-R	**50 °C**	X	X	X	X	X	X	X

The stress-strain curves were used to calculate average material parameters such as ultimate tensile strength and elastic modulus. Anand parameters were experimentally obtained and fitted using the non-linear least squares fitting method. The results were then compared with the predicted stress-strain curve generated by the Anand model. In order to fit the material data to the Anand Viscoplasticity model, nine Anand constants were derived for various SAC solders.

ANAND VISCOPLASTIC CONSTITUTIVE MODEL

Anand model [17]- [19] is widely used for non-linear solder alloys. The model employs flow, evolution, and stress equations to describe the rate-dependent plastic behavior of the solder alloy. For one-dimensional uniaxial tensile loading, the stress equation can be defined as:

$$\sigma = \frac{1}{\xi}\sinh^{-1}\left\{\left[\frac{\dot{\varepsilon}_p}{A}\exp\left(\frac{Q}{RT}\right)\right]^m\right\} \left\{\hat{s}\left[\frac{\dot{\varepsilon}_p}{A}\exp\left(\frac{Q}{RT}\right)\right]^n + \left\{\left(\hat{s}\left[\frac{\dot{\varepsilon}_p}{A}\exp\left(\frac{Q}{RT}\right)\right] - s_0\right)^{1-a} + \left\{(a-1)\left[h_0\left(\hat{s}\left[\frac{\dot{\varepsilon}_p}{A}\exp\left(\frac{Q}{RT}\right)\right]^n\right)\right]^{-a}\varepsilon_p\right\}^{1/1-a}\right\}\right\} \quad (1)$$

Where σ represents stress, s represents an internal variable, and c is a function of the strain rate ($\dot{\varepsilon_p}$), ξ denotes the stress multiplier, T represents the temperature in Kelvin, A is the pre-exponential factor, Q is the activation energy, R is the universal gas constant, and m represents the sensitivity of the strain rate. Equation (1) consists of a total of 9 constants of the material: *A, ξ, Q/R, h_0, m, s_0, $\hat{s}$* and *a*. By assuming that ε_p approaches infinity, the ultimate tensile strength (UTS) can be determined.

$$\sigma^* = UTS = \sigma\Big|_{\varepsilon_p \to \infty} \tag{2}$$

$$\therefore \sigma^* = \frac{\hat{s}}{\xi}\left[\frac{\dot{\varepsilon}_p}{A}\exp\left(\frac{Q}{RT}\right)\right]^n \sinh^{-1}\left\{\left[\frac{\dot{\varepsilon}_p}{A}\exp\left(\frac{Q}{RT}\right)\right]^m\right\}$$

To provide further simplification, upon substituting this value of UTS back into equation (1), the resulting expression is as follows:

$$\sigma = \sigma^* - [(\sigma^* - cs_0)^{1-a} + (a-1)\{ch_0(\sigma^*)^{-a}\}\varepsilon_p]^{1/1-a} \tag{3}$$

Where, c is a function of strain rate:

$$c = (\dot{\varepsilon}_p, T) = \frac{1}{\xi}\sinh^{-1}\left\{\left[\frac{\dot{\varepsilon}_p}{A}\exp(\frac{Q}{RT})\right]^m\right\} \tag{4}$$

Several tensile tests were conducted over a range of operating temperatures (-65 to 200°C) and strain rates (10, 35, 50, 75 per second) to determine the 9 constants of the Anand viscoplasticity Model. The results of the experiments were then analyzed using MATLAB's least square non-linear algorithm. These nine constants are *A, a, Q/R, ξ, h_0, m, n, ŝ* and *s_0* are determined as follows:

(i) Experimental results of ultimate stress were fit using equation (2) and the values of parameters *A, Q/R, m, n,* and $\hat{s}/\xi$ are calculated.

(ii) As $\hat{s}/\xi$ value is obtainable from the previous step, *ξ* is designated in a way that *σ/s* ratio is less than unity. Then $\hat{s}$ is calculated using the term $\hat{s}/\xi$, calculated in the first step.

(iii) Plastic strain is to be fitted to all the temperatures and strain rates using equation (2), calculating the values of parameters *a, h_0,* and *S_0*.

Table 3. Anand Parameters for SAC-Q: Aged at 50 °C.

Anand Constant	0 Days	30 Days	60 Days	120 Days	180 Days	270 Days	360 Days
A	5143	6005	6572	6964	7245	8023	8463
ξ	4.28	4.28	4.28	4.28	4.28	4.28	4.28
Q/R	8444	8644	8644	8644	8644	8644	8644
a	1.2	1.28	1.32	1.35	1.40	1.42	1.44
h_0	110353	100264	93765	91828	88364	87955	80880
m	0.59	0.52	0.47	0.43	0.41	0.36	0.3
n	0.0075	0.0059	0.0051	0.0046	0.0043	0.0040	0.0026
ŝ	48.56	34.86	30.52	28.5	26.6	24.2	22.4
s_0	1.99	1.75	1.7	1.68	1.63	1.59	1.44

The model constants included in Table 3 to Table 6 illustrate the behavior of all four materials at all test temperatures and strain rates for various aging durations. Fig. 1 to Fig. 4 compare experimental and model-predicted curves for the SAC305, SAC-Q, M758, and SAC-R, and they show a strong correlation. Each curve is the mean of five different curves. For model curves, the stress-strain data have been fitted using MATLAB using equations (2) and (3). Fig. 1 to Fig. 4 show curves with solid lines representing experimental data and dotted lines representing curves predicted by the Anand model. According to prior research [7]- [15], SAC solder materials are temperature and strain-rate-sensitive. Data shows that the solder materials tested increased in the ultimate tensile strength with the decrease in operating temperature to -65°C from +200°C.

Table 4. Anand Parameters for SAC305: Aged at 100 °C.

Anand Constant	0 Days	30 Days	60 Days	120 Days	180 Days	240 Days	360 Days
A	650	730	762	800	862	920	960
ξ	6.7	6.7	6.7	6.7	6.7	6.7	6.7
Q/R	4500	4500	4500	4500	4500	4500	4500
a	1.16	1.2	1.26	1.34	1.368	1.371	1.38
h_0	163700	108000	91860	91400	86100	81305	73375
m	0.4637	0.4401	0.4213	0.361	0.349	0.3106	0.30
n	0.0055	0.0056	0.00551	0.00526	0.00699	0.0078	0.014
ŝ	64.176	56.322	48.54	50.85	41.10	39.07	31.89
s_0	0.294	0.29	0.279	0.243	0.239	0.18	0.09

Table 5. Anand Parameters for M758: Aged at 100 °C.

Anand Constant	0 Days	30 Days	180 Days	360 Days
A	6125	6300	6700	7050
ξ	1.8	1.8	1.8	1.8
Q/R	9000	9000	9000	9000
a	1.106	1.149	1.18	1.21
h_0	98802	92055	87906	84300
m	0.05268	0.0466	0.0433	0.04
n	0.0122	0.0089	0.0012	0.001
ŝ	63.55	61.04	57.11	50.44
s_0	0.455	0.28	0.347	0.176

Table 6. Anand Parameters for SAC-R: Aged at 50 °C.

Anand Constant	0 Days	30 Days	60 Days	120 Days
A	1028	1010	3835	2412
ξ	4	4	4	4
Q/R	7626	7626	7626	7626
a	1.01	1.01	1.01	1.01
h_0	76540	94650	82350	62350
m	0.3012	0.2783	0.3944	0.2154
n	3.32e-14	2.309e-14	3.279e-14	5.33e-14
ŝ	38.118	38.692	28.716	25.716
s_0	3.408e-15	9.761e-12	2.27e-08	8.7e-07

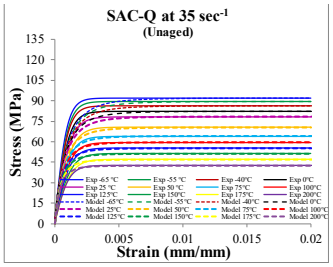

Fig. 1. SAC-Q Anand Model vs Expts at $\dot{\varepsilon}$ = 35s^{-1} (Pristine)

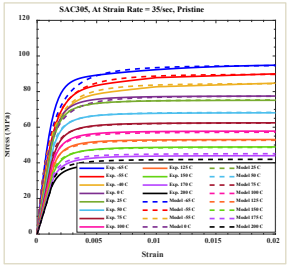

Fig. 2. SAC305Anand Model vs Expts at $\dot{\boldsymbol{\varepsilon}}$ = 35s^{-1} (Pristine)

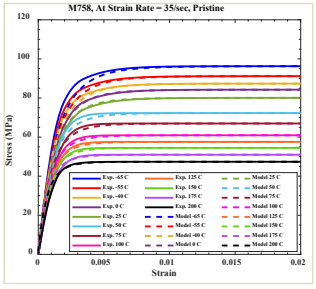

Fig. 3. M758 Anand Model vs Expts at $\dot{\boldsymbol{\varepsilon}}$ = 35s^{-1} (Pristine)

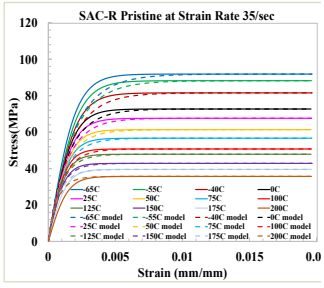

Fig. 4. SAC-R Anand Model vs Expts at $\dot{\boldsymbol{\varepsilon}}$ = 35s^{-1} (Pristine)

The Ultimate Tensile Strength (UTS) increased as the strain rate went up, regardless of the operating temperature within the range of -65°C to +200C. This was observed for all solder alloys investigated. Using experimental results from 12 different operating temperatures and four strain rates, the nine Anand parameters were computed, resulting in a better prediction of the stress-strain curve for temperatures in the center range. However, for upper and lower temperatures, the predicted curve showed a higher variation from the experimental data. Less error was found for all solder materials in the center range of operating temperatures (50-125°C). The Anand Model predicts viscous plasticity, and both temperature and strain rate affect material deformation behavior. The authors suggest that it is possible to minimize deviation for temperatures at the upper or lower end of the operating range by adjusting the model constants.

THERMAL AGING EFFECTS

The following section discusses the impact of thermal aging on solder alloys. The solders namely SAC-Q and SAC-R were thermally aged at 50°C while SAC305 & M758 were aged at 100°C for up to 1 year. The study examined the effect of thermal aging on UTS & E for all four solders, as shown in Fig. 5 to Fig. 12. The research findings revealed that mechanical characteristics deteriorated with longer thermal aging time at all strain rates and operating temperatures. Specifically, the values of E and UTS dropped with an increase in thermal aging time.

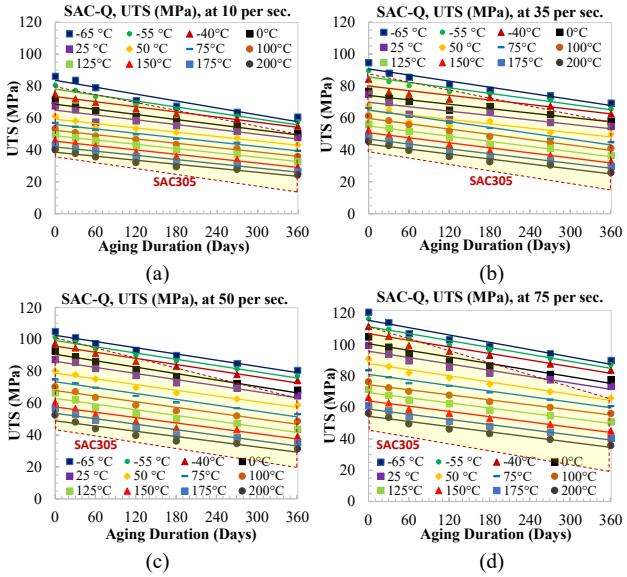

Fig. 5. UTS vs Thermal Aging for SAC-Q, aged at 50 °C: (a) 10 s^{-1}, (b) 35 s^{-1}, (c) 50 s^{-1}, (d) 75 s^{-1}

The data presented in Fig. 5 and Fig. 6 reveal that the highest UTS and E values were observed at a temperature of -65°C and a strain rate of 75 per sec, while the lowest values were recorded at a temperature of +200°C and a strain rate of 10 per sec for all solders. Linear degradation was observed in both mechanical properties due to aging, with the properties of SAC305 decreasing as the aging period increased from 0 to 360 days, similar to the SAC-Q solder. The results show a decline in UTS and E values after thermal aging. For thermal-aged SAC305, Fig. 7 and Fig. 8 demonstrate how UTS and E values decrease with increased test temperatures for different strain rates. Meanwhile, Fig. 9 to Fig. 12 show the aging effect on M758 and SAC-R solder for up to 1 year of aging and operating temperatures ranging from -65 to +200°C on UTS and E, at strain rates of 10 to 75 per sec. The aging effect on all four SAC solder materials exhibited similar patterns.

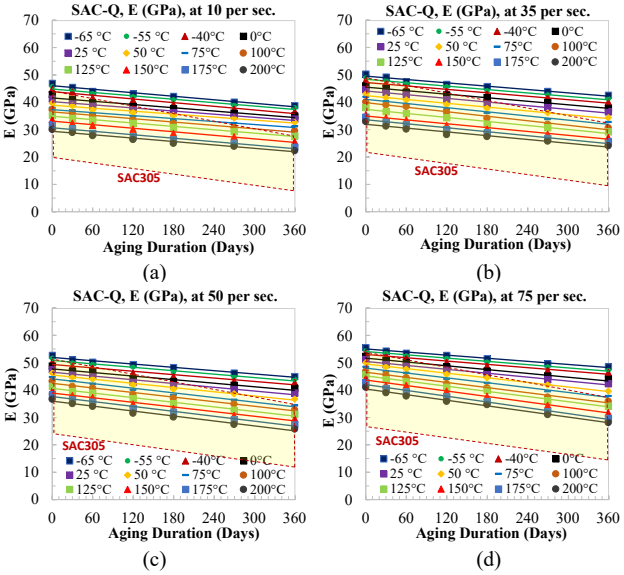

Fig. 6. E vs Thermal Aging for SAC-Q, aged at 50 °C: (a) 10 s^{-1}, (b) 35 s^{-1}, (c) 50 s^{-1}, (d) 75 s^{-1}

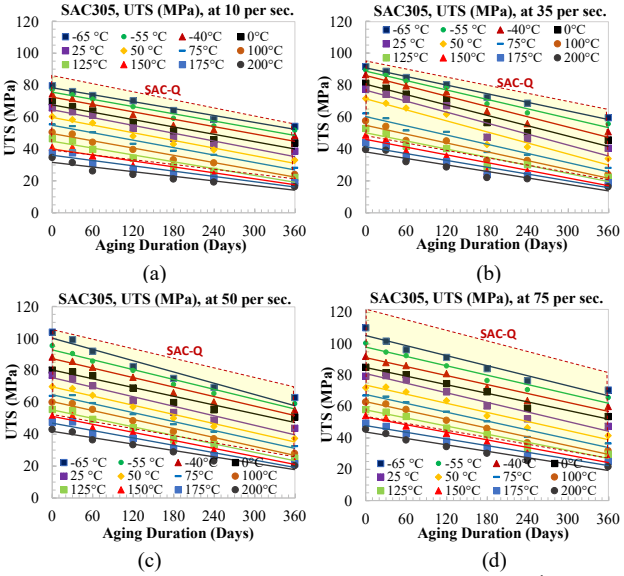

Fig. 7. UTS for SAC305, aged at 100 °C(a)10 s^{-1} (b)35 s^{-1} (c)50 s^{-1} (d)75 s^{-1}

Research has shown that SAC solder with bismuth content is less sensitive to thermal aging duration and operating temperature when compared to traditional SAC305 solder. Higher material property values were observed for M758 and SAC-Q solder when compared to SAC305 and SAC-R. Among different solder alloys tested under various aging conditions, M758 performed the best. This could be due to the presence of Ni and Bismuth content in M758 solder alloy. Wu [20] and Hassan [21] reported that the microstructure of SAC-Q solder alloy grew in various aging durations.

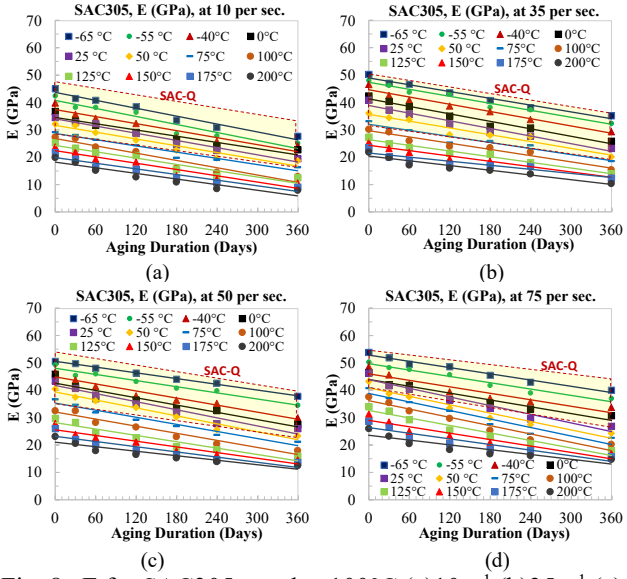

Fig. 8. E for SAC305, aged at 100°C (a)10 s^{-1} (b)35 s^{-1} (c)50 s^{-1} (d) 75s^{-1}

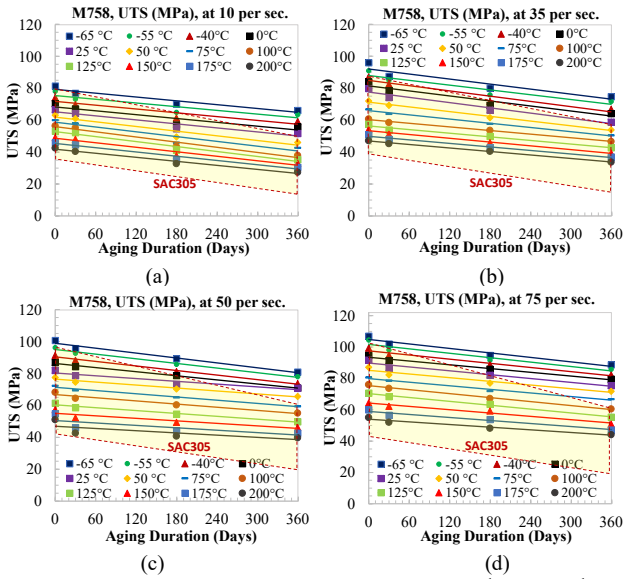

Fig. 9. UTS for M758, aged at 100°C: (a)10 s^{-1} (b)35 s^{-1} (c)50 s^{-1} (d)75 s^{-1}

It was observed that the average particle diameter of SAC-Q increased by over 100% during aging, which is less than the particle increments of 300% observed for SAC305. In SAC-Q solder alloy, IMC particle coarsening was significantly mitigated compared to SAC305. Bismuth was observed during aging in the beta-Sn dendrites and in the rich intermetallic regions between dendrites. A solid solvent reinforced the lead-free solder. The presence of bismuth in SAC-Q base increases the resistance to diffusion of Ag_3Sn IMC particles [20]. When compared to SAC305 under the same operating temperature conditions ranging from -65°C to +200°C, the elastic modulus and ultimate tensile strength of the SAC-R solder degrade to a lesser degree.

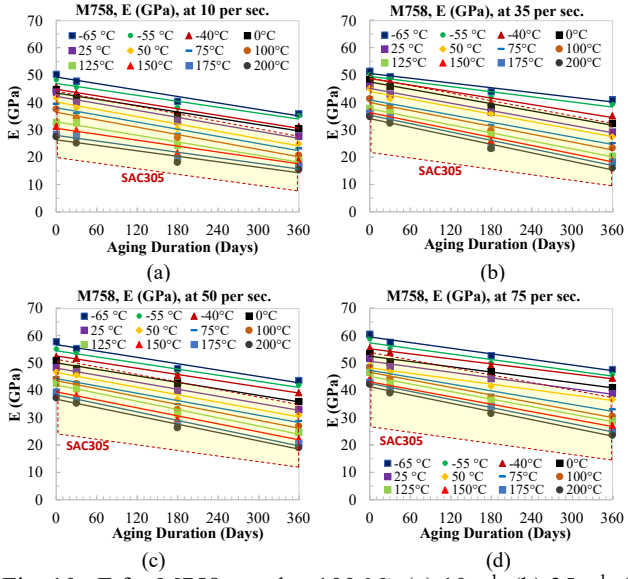

Fig. 10. E for M758, aged at 100 °C: (a) 10 s^{-1}, (b) 35 s^{-1}, (c) 50 s^{-1}, (d) 75 s^{-1}

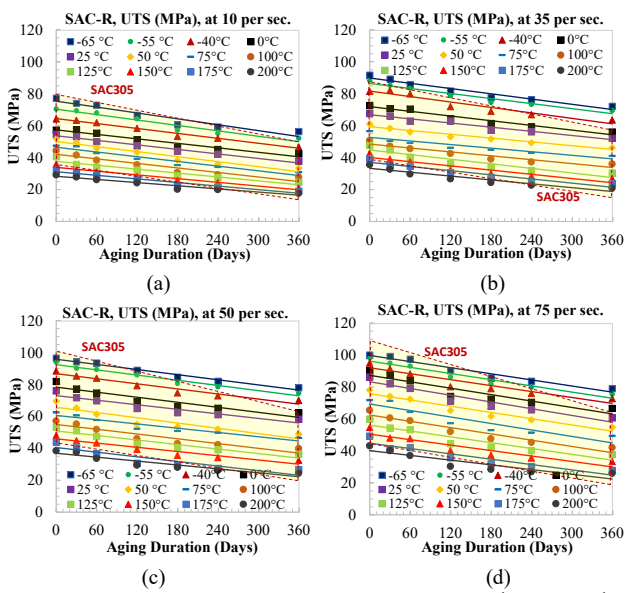

Fig. 11. UTS for SAC-R, aged at 50°C (a)10 s^{-1}, (b)35 s^{-1}, (c) 50 s^{-1}, (d)75 s^{-1}

Furthermore, the temperature dependence of SAC-R's constitutive behavior versus SAC305 is lower at all strain rates between 1-100s^{-1} and exposure durations of time-temperature sustained exposure. The muted dependence of elastic modulus can be easily observed in the lower spread of the curves in Fig. 12. The amount of bismuth present in the SAC+X alloy was found to be directly proportional to the resistance to aging and the increase in mechanical properties [20]. Thus, higher percentages of Bismuth in the range of alloys examined had a positive effect on the mitigation of harmful effect of thermal aging in the SnAgCu solder alloys under operation at high strain rates.

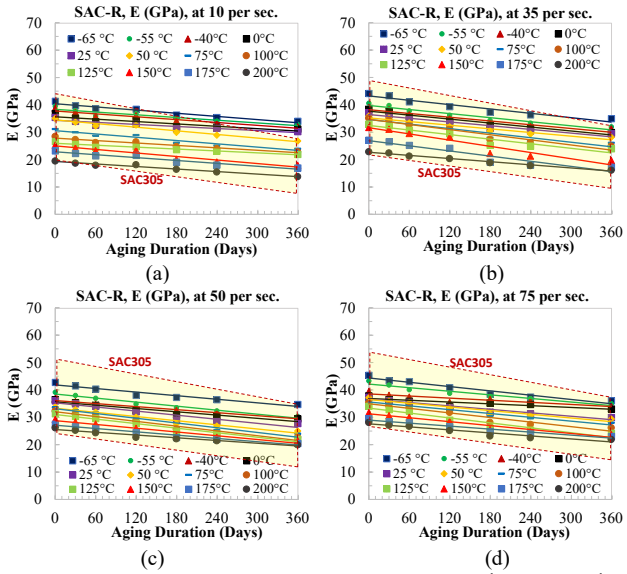

Fig. 12. E for SAC-R, aged at 50°C: (a) 10 s^{-1}, (b) 35 s^{-1}, (c) 50 s^{-1}, (d) 75 s^{-1}

DROP TEST SIMULATION

In order to assess the capabilities of the Anand constitutive model, ANSYS was used to conduct a simulation of a drop event through finite element analysis (FEA). Using the input-G method, hysteresis loops and plastic work were extracted from the simulated drop event. To analyze the damage trend in each solder connection, the hysteresis loop and plastic work density were retrieved at various temperatures under high-g shock. The test vehicle depicted in Fig. 13 features a center-mounted PBGA324 package, with a test board measuring 132 mm x 77 mm x 1.5 mm and featuring a 1 mm pitch and 324 I/O counts for solder balls. To capture the transient mode shapes, ANSYS was used to design a test vehicle with a center-mounted PBGA324 package. The ANSYS model for the drop event test vehicle is shown in Fig. 14.

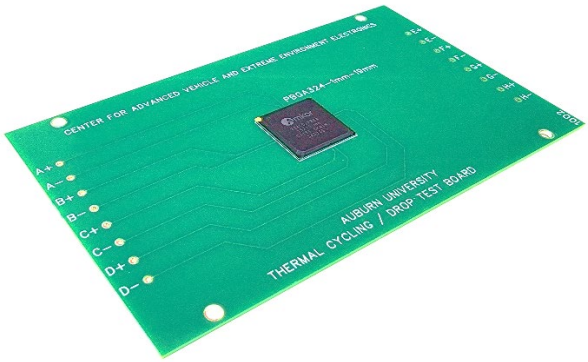

Fig. 13. Test Board with PBGA324 Package.

The critical/corner solder balls are represented by the VISCO107 elements, while the Timoshenko beam elements represent the remaining solder junctions and are represented by BEAM188 components. The SOLID45 components consist of the PCB and other package components. The package assembly includes solder joints, Mold compound, silicon die, die attach, BT substrate, copper pad, and PCB. The Poisson's Ratio for each part ranges from 0.28 to 0.39, and the density for each part ranges from 8.82E-09 to 1.65E-09. The values of E for solder joints were obtained through experimentation under specific conditions and strain rates, while the values of E for other parts of the package assembly range from 2760 MPa to 162000 MPa and were taken from previously published literature.

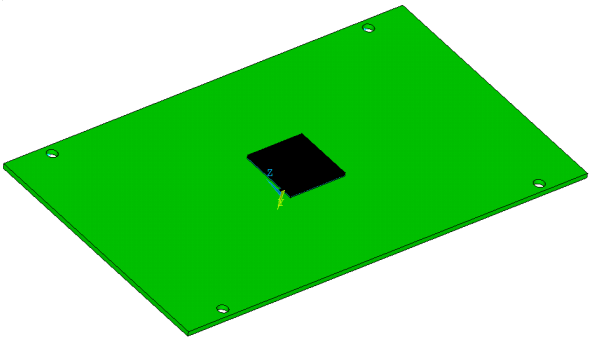

Fig. 14. Modeled PCB- PBGA324 Package assembly.

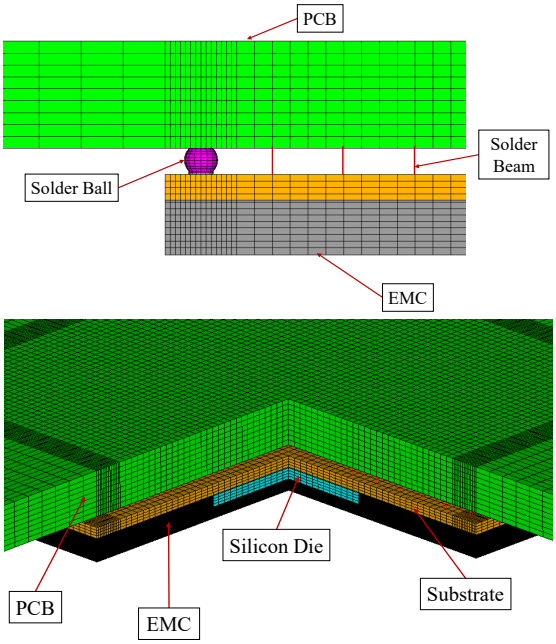

Fig. 15. Cut-Section view of package.

In Fig. 15, a cut-view of a test vehicle component is displayed as a mesh. To utilize the input-G method, four mass components were created at the center of the PCB screw holes, each with a weight five orders of magnitude heavier than the actual weight of the test board. These components were then firmly attached to the PCB using a stiff element. The input acceleration was applied to the mass node, and the input force was calculated by multiplying the mass of the mass node with the input acceleration. To simulate the drop event, a half-sine shock pulse of 1500g and 0.5ms was employed. The tabular force data served as a boundary condition to apply the appropriate acceleration to the mass elements in the test board. Finally, the shock-impact problem was resolved using the preconditioned gradient solution.

Stress Distribution

FEA-based modeling was used to establish the stress distribution for the critical solder joint. The critical solder connection is located near the corner of the package, and the

simulation has provided us with the stresses and strains for this connection. The stress contour plot in the y-direction (σ_y) for the critical solder junction is shown in Fig. 16. The highest observed stress was found in both the solder connection and the copper pad.

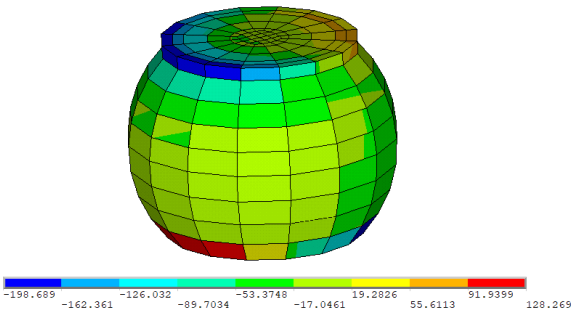

Fig. 16. Solder Joint Stress Distribution (Contour Plot).

Hysteresis Loop and Plastic Work Density

FEA-based simulation using volume average technique was employed to retrieve plastic work densities and stress-strain results of the critical solder ball. This technique helps to minimize the impact of mesh density on finite element results. The top layer of the essential solder ball was used to calculate the average plastic work values.

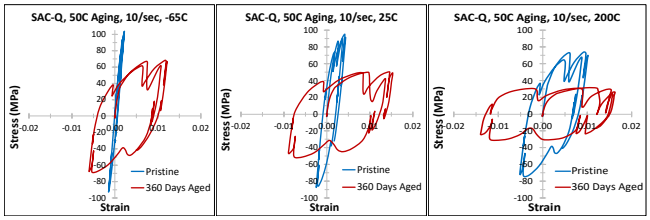

(a) (b) (c)

Fig. 17. Hysteresis Loops for Pristine and 360 days aged SAC-Q Solder Alloy: (a) -65ºC, (b) 25ºC, (c) at 200ºC

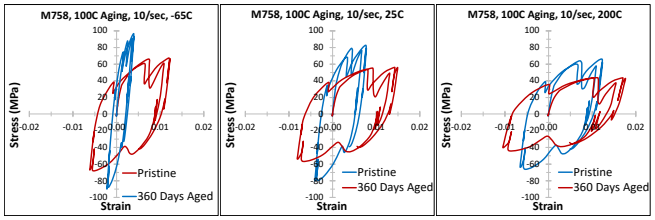

(a) (b) (c)

Fig. 18. Hysteresis Loops for Pristine and 360 days aged M758: (a) -65ºC, (b) 25ºC, (c) at 200ºC

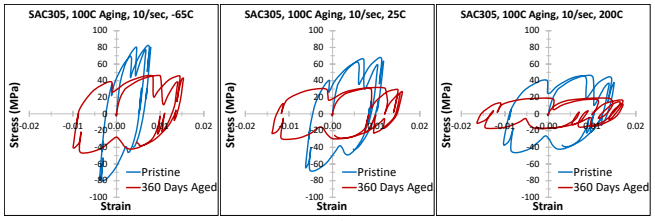

(a) (b) (c)

Fig. 19. Hysteresis Loops for pristine and 360 days aged SAC305: (a) -65ºC, (b) 25ºC, (c) at 200ºC

For the critical solder ball layer shown in Fig. 16 the stress-strain data are extracted in the y direction to represent the hysteresis loop for SAC solder alloys at operating temperatures of -65°C, 25°C, and 200°C as shown in Fig. 17 to Fig. 20. According to results, peak stress levels fall as operational temperatures rise. The hysteresis loop area increased for all solder alloy as the aging duration increased from pristine to up to one year.

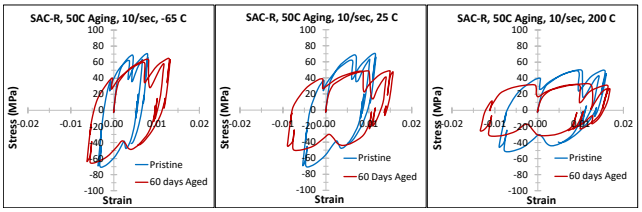

(a) (b) (c)

Fig. 20. Hysteresis Loops for Pristine and 60 days aged SAC-R Solder for: (a) at -65ºC, (b) 25ºC, (c) at 200ºC

EFFECT OF BISMUTH ON AGING DEGRADATION

Fig. 21 shows the degradation rate in the ultimate tensile strength in MPa/Month versus Bismuth content at various operating temperatures. SAC305 has no Bismuth, M758 has 4 percent Bismuth, and SAC-Q has 4.9 percent Bismuth. Thus, an increase in the Bismuth content reduces the degradation rate of the UTS per month that is realized at any operating temperature in the range of -65°C to +200°C for all strain rates measured, including $10s^{-1}$, $35s^{-1}$, $50s^{-1}$, and $75s^{-1}$.

	SAC305	SAC-Q	M758
Bismuth %	0.0	3.0	4.0

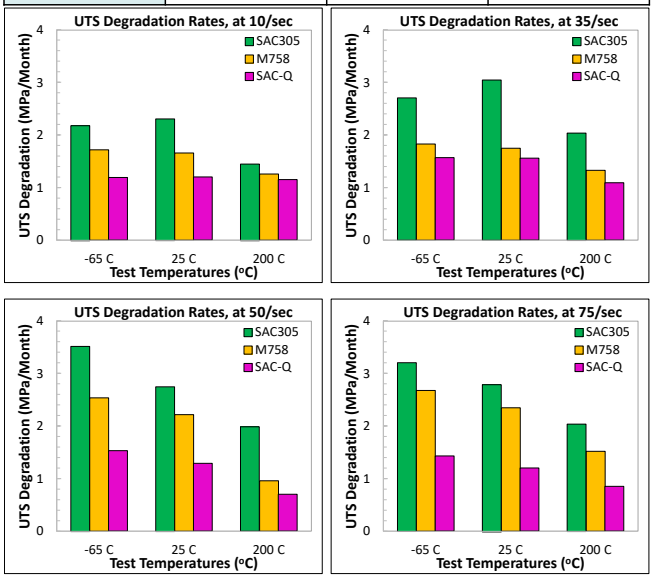

Fig. 21. Degradation Rate of UTS vs Bismuth Content at various Operating Temperatures

SUMMARY AND CONCLUSIONS

This research delves into the effects of low working temperatures and high strain rates on mechanical parameters, including ultimate tensile strength (UTS) and elastic modulus (E), in un-doped and doped solders. Samples of unaged and isothermally aged solder were tested using high strain rate tensile tests across a range of temperatures (-65 to 200°C). The results showed that the elastic modulus and UTS of all SAC solders are dependent on strain rate and increase as strain rate increases. Interestingly, all SAC solders exhibit

increased mechanical characteristics at -65°C. The study also examined the impact of thermal aging on various solder alloys at low working temperatures. The results showed that isothermal aging has less of an impact on the material characteristics of certain solders compared to others. In addition, the study found that the impact of operating temperature is greater than that of thermal aging for all the solder alloys examined. To predict stress-strain curves, the study derived 9 Anand parameters from the stress-strain data and fitted the experimental material data to the Anand viscoplasticity constants using the non-linear least squares technique. The stress-strain curves from Anand constants had a good correlation with the experimental data. The study also used ANSYS™ software to evaluate a drop event based on FEA. The results showed that the solder junction and copper pad experienced the greatest amount of stress during the drop event. Plastic work in the solder joints was evaluated using an FEA-based drop simulation at 1500g for extremely high ambient temperatures. The study also determined the evolution of the hysteresis loop and plastic work density due to thermal aging.

ACKNOWLEDGMENTS

The research results presented in this paper have been supported by a grant from the National Science Foundation and members of NSF-CAVE3 Electronics Research Center.

REFERENCES

[1] D. S. Eddy and D. R. Sparks, "Application of MEMS technology in automotive sensors and actuators," in Proceedings of the IEEE, vol. 86, no. 8, pp. 1747-1755, Aug. 1998.

[2] M. Hattori, "Needs and applications of high temperature LSIs for automotive electronic systems," HITEN 99. Third European Conference on High Temperature Electronics. (IEEE Cat. No.99EX372), Berlin, Germany, 1999, pp. 37-43.

[3] R. W. Johnson, J. L. Evans, P. Jacobsen, J. R. Thompson and M. Christopher, "The changing automotive environment: high-temperature electronics," in IEEE Transactions on Electronics Packaging Manufacturing, vol. 27, no. 3, pp. 164-176, July 2004.

[4] M. Basit, M., Motalab, J. C., Suhling, & P., Lall, (2014, May). The effects of aging on the Anand viscoplastic constitutive model for SAC305 solder. In Thermal and Thermomechanical Phenomena in Electronic Systems (ITherm), 2014 IEEE Intersociety Conference on (pp. 112-126). IEEE.

[5] Z. Cai, Y. Zhang, J. C. Suhling, P. Lall, R. W. Johnson and M. J. Bozack, "Reduction of lead free solder aging effects using doped SAC alloys," 2010 Proceedings 60th Electronic Components and Technology Conference (ECTC), Las Vegas, NV, 2010, pp. 1493-1511.

[6] Motalab, M., Z. Cai., J. Suhling, J. Zhang, J. Evans, M. Bozack, P. Lall. Improved Prediction of Lead Free Solder Joint Reliability that Include Aging Effect, Proceedings of the 62nd ECTC, pp 513-531, May 29-June 1, San Diego, CA 2012.

[7] P. Lall, D. Zhang, V. Yadav, and D. Locker, "High strain rate constitutive behavior of SAC105 and SAC305 leadfree solder during operation at high temperature," Microelectronics Reliability, Volume 62, 2016, Pages 4-17.

[8] P. Lall, D. Zhang, V. Yadav, J. Suhling and D. Locker, "Effect of Prolonged Storage up to 1-Year on the High Strain Rate Properties of SAC Leadfree Alloys at Operating Temperatures up to 200 °C," 2017 IEEE 67th Electronic Components and Technology Conference (ECTC), Orlando, FL, 2017, pp. 1219-1230.

[9] P. Lall, V. Yadav, V. Mehta, J. Suhling and K. Blecker, "Extreme Cold-Temperature High-Strain Rate Properties of SAC Solder Alloys," 2020 IEEE 70th Electronic Components and Technology Conference (ECTC), Orlando, FL, USA, 2020, pp. 782-792.

[10] P. Lall, V. Yadav, J. Suhling and D. Locker, "Low Temperature High Strain Rate Material Properties for SAC-Q Leadfree Alloys," 2020 19th IEEE Intersociety Conference on Thermal and Thermomechanical Phenomena in Electronic Systems (ITherm), Orlando, FL, USA, 2020, pp. 1084-1099.

[11] P. Lall, V. Mehta, J. Suhling and K. Blecker, "High Strain-Rate Properties for SAC305 at Cold Operating Temperatures down to -65°C," 2020 19th IEEE Intersociety Conference on Thermal and Thermomechanical Phenomena in Electronic Systems (ITherm), Orlando, FL, USA, 2020, pp. 1073-1083.

[12] P. Lall, V. Mehta, J. Suhling and K. Blecker, "Low-Temperature High Strain Rate Constitutive Behavior of Doped and Undoped SnAgCu Solder Alloys after Prolonged Storage at High Temperature," 71st Electronic Components and Technology Conference (ECTC), pp. 448-459, 2021.

[13] P. Lall, V. Mehta, J. Suhling and K. Blecker, "High Strain Rate Properties of M758 Solder at Extreme Operating Temperatures", 20th IEEE Intersociety Conference on Thermal and Thermomechanical Phenomena in Electronic Systems (iTherm), pp. 830-841, 2021.

[14] P. Lall, V. Mehta, J. Suhling and K. Blecker, "Effect of Evolution of High Strain Rate Properties on Plastic-Work of SAC305 Alloy with 100°C Aging for Periods up to 240-days," 2022 21st IEEE Intersociety Conference on Thermal and Thermomechanical Phenomena in Electronic Systems (iTherm), San Diego, CA, USA, 2022, pp. 1-16.

[15] P. Lall, V. Mehta, J. Suhling and K. Blecker., "High Strain Rate Mechanical Properties of SAC-Q Solder for Extreme Temperatures After Exposure to Isothermal Aging Up to 90 Days", Journal of Electronic Packaging, Vol. 144(2), 2022.

[16] Wong, E., H., Selvanayagam, C.,S., Seah, S.,K.,W., Driel, W.,D., Caers, J.,F.,J.,M., Zhao, X.,J., Owens,N., Tan, L.,C., Frear, D.,R. , Leoni, M. , Lai, Y.,S., Yeh, C.,-L., "Stress–strain characteristics of tin-based solder alloys at medium strain rate," Materials Letters 62,pp.3031–3034, 2008.

[17] L. Anand, "Constitutive Equations for the Rate-Dependent Deformation of Metals at Elevated Temperatures," Journal of Engineering Materials and Technology, Vol. 104(1), pp. 12-17, 1982.

[18] N. Bai, C. Xu, and G. Hong, "Simulation of uniaxial tensile properties for lead-free solders with modified

Anand model." Materials & Design 30, no. 1 (2009): 122-128.
[19] Amagai, M., Watanabe, M., Omiya, M., Kishimoto, K., and Shibuya, T., "Mechanical Characterization of Sn-Ag Based Lead-Free Solders," Microelectronics Reliability, Vol. 42(6), pp. 951-966, 2002.
[20] J. Wu, S. Ahmed, J. C. Suhling and P. Lall, "Investigation of Aging Induced Microstructural Changes in Doped SAC+X Solders," 2019 18th IEEE Intersociety Conference on Thermal and Thermomechanical Phenomena in Electronic Systems (ITherm), Las Vegas, NV, USA, 2019, pp. 405-415.
[21] K. R. Hassan, J. Wu, M. S. Alam, J. C. Suhling and P. Lall, "Mechanical Behavior and Reliability of SAC+Bi Lead Free Solders with Various Levels of Bismuth," 2021 IEEE 71st Electronic Components and Technology Conference (ECTC), 2021, pp. 937-945